Astronomy & Astrophysics manuscript no. PACWB_Neiner
January 18, 2021
©ESO 2021

arXiv:1412.5327v1 [astro-ph.SR] 17 Dec 2014

Search for magnetic fields in particle-accelerating colliding-wind binaries⋆

C. Neiner[1], J. Grunhut[2], B. Leroy[1], M. De Becker[3], and G. Rauw[3]

[1] LESIA, Observatoire de Paris, CNRS UMR 8109, UPMC, Université Paris Diderot, 5 place Jules Janssen, 92190 Meudon, France; e-mail: coralie.neiner@obspm.fr
[2] European Southern Observatory (ESO), Karl-Schwarzschild-Str. 2, 85748, Garching, Germany
[3] Department of Astrophysics, Geophysics and Oceanography, University of Liège, 17 Allée du 6 Août, B5c, 4000, Sart Tilman, Belgium

Received ...; accepted ...

ABSTRACT

Context. Some colliding-wind massive binaries, called particle-accelerating colliding-wind binaries (PACWB), exhibit synchrotron radio emission, which is assumed to be generated by a stellar magnetic field. However, no measurement of magnetic fields in these stars has ever been performed.
Aims. We aim at quantifying the possible stellar magnetic fields present in PACWB to provide constraints for models.
Methods. We gathered 21 high-resolution spectropolarimetric observations of 9 PACWB available in the ESPaDOnS, Narval and HarpsPol archives. We analysed these observations with the Least Squares Deconvolution method. We separated the binary spectral components when possible.
Results. No magnetic signature is detected in any of the 9 PACWB stars and all longitudinal field measurements are compatible with 0 G. We derived the upper field strength of a possible field that could have remained hidden in the noise of the data. While the data are not very constraining for some stars, for several stars we could derive an upper limit of the polar field strength of the order of 200 G.
Conclusions. We can therefore exclude the presence of strong or moderate stellar magnetic fields in PACWB, typical of the ones present in magnetic massive stars. Weak magnetic fields could however be present in these objects. These observational results provide the first quantitative constraints for future models of PACWB.

Key words. stars: magnetic fields - stars: early-type - binaries: spectroscopic - stars: individual: HD 36486, HD 37468, HD 47839, HD 93250, HD 151804, HD 152408, HD 164794, HD 167971, HD 190918

1. Introduction

Colliding-wind massive binaries (CWB) are binary systems composed of two stars of O, early-B or WR type. Their main feature is a wind-wind interaction region where the shocked gas is very hot (10^7 K). This wind interaction region is likely to contribute to the thermal radio emission, in addition to the free-free radiation due to thermal electrons in single star winds (Dougherty et al. 2003).

In addition to this thermal emission, non-thermal radio emission was discovered in some systems. It is related to the synchrotron radiation due to the presence of relativistic electrons (Pittard et al. 2006). These synchrotron emitters are called particle-accelerating colliding-wind binaries (PACWB). In addition to the synchrotron emission, these systems can be revealed by exceptionally large radio fluxes, a spectral index significantly lower than the thermal value, and an orbital modulation of the radio flux. De Becker & Raucq (2013) recently provided the most up-to-date catalog of such systems.

High angular resolution observations of some PACWB have allowed to disentangle the thermal and non-thermal emissions (e.g. OB2 #5, Dzib et al. 2013) and showed that the synchrotron emission is associated to the wind-wind interaction region. This region is also a source of thermal X-rays, in addition to the intrinsic X-ray emission produced in the stellar winds of the individual components. The X-ray spectrum produced in the wind interaction region is generally significantly harder than that of massive single stars, and the X-ray emission is variable with the orbital phase (e.g. De Becker et al. 2011; Cazorla et al. 2014).

Finally, it was discovered more recently that PACWB may also emit γ rays through inverse Compton scattering by the relativistic electrons and neutral pion decay. However, only one such example is known as of today (η Car, Farnier et al. 2011).

These many characteristics make PACWB very interesting objects to study extreme physical processes. However, it has become more and more clear over the last few years that PACWB cover a very wide range of parameters (mass loss, wind velocity, orbital period...) and the fundamental difference between the PACWB and "normal" CWB is unknown (De Becker & Raucq 2013).

The presence of synchrotron emission in PACWB immediately points towards the presence of a magnetic field. Indeed,

Send offprint requests to: C. Neiner

⋆ Based on archival observations obtained at the Telescope Bernard Lyot (USR5026) operated by the Observatoire Midi-Pyrénées, Université de Toulouse (Paul Sabatier), Centre National de la Recherche Scientifique (CNRS) of France, at the Canada-France-Hawaii Telescope (CFHT) operated by the National Research Council of Canada, the Institut National des Sciences de l'Univers of the CNRS of France, and the University of Hawaii, and at the European Southern Observatory (ESO), Chile.

synchrotron emission results from the modified movement of relativistic electrons in a magnetic field. Moreover, the acceleration of particles in PACWB could be explained either by strong shocks in the colliding winds (e.g. Pittard et al. 2006) or by magnetic reconnection or annihilation (e.g. Jardine et al. 1996). It has thus been speculated that the fundamental difference between CWB and PACWB is the presence of a magnetic field.

Over the last two decades magnetic fields have been detected in ∼7% of single massive stars (Wade et al. 2014b). While the fraction of PACWB among CWB is not known and the catalog by De Becker & Raucq (2013) certainly underestimates the number of PACWB, ∼7% could be a plausible proportion considering that only 43 possible PACWB have been identified as of today (De Becker & Raucq 2013) while most massive stars are probably in binaries (Sana et al. 2012, 2014). Therefore, the presence of a magnetic field might indeed be the difference between PACWB and "normal" CWB.

The magnetic field in PACWB could be of stellar origin or it could also possibly be generated in the colliding winds themselves. From synchrotron observations, one can estimate the magnetic field strength in the wind-wind interaction region to be of the order of a few mG (see e.g. Dougherty et al. 2003). Extrapolating to the surface of the stars with typical distances between the stagnation point and the photosphere, we obtain values of the stellar magnetic field strength between one G and a few thousands G, depending on the system and on the assumptions (e.g. Parkin et al. 2014). Magnetic fields detected in single massive stars have a polar field strength between hundred and several thousands G (see e.g. Petit et al. 2013), which are compatible with the fields speculated in PACWB models.

Therefore, measuring magnetic fields in PACWB is an ideal way to test these assumptions, constrain models of colliding winds, and understand the difference between PACWB and "normal" CWB.

2. Archival spectropolarimetric observations

An updated census of 43 PACWB has been published recently (De Becker & Raucq 2013). It includes clear PACWB detected through their synchrotron emission as well as candidates from indirect indicators (e.g. radio flux).

We have gathered all high-resolution spectropolarimetric data of these PACWB available in archives, i.e. observed with Narval at Télescope Bernard Lyot (TBL) in France, ESPaDOnS at the Canada-France-Hawaii telescope (CFHT) in Hawaii, or HarpsPol at ESO in Chile. Circular polarisation data are available for 9 of the 43 known PACWB. When several consecutive spectra were available for the same night, we averaged them. The 9 stars and 21 (average) observations are listed in Table 1.

For each star, we normalized the data to the intensity continuum level and extracted Stokes *V* and Null (*N*) polarisation spectra. *N* spectra allow us to check that the magnetic measurements (in the Stokes *V* spectra) have not been polluted by spurious signal, e.g. due to instrumental polarisation.

We then proceeded to use the Least Squares Deconvolution (LSD) technique (Donati et al. 1997) to search for weak Zeeman signatures in the mean Stokes *V* profile. The input LSD masks for each star were extracted from line lists provided by VALD (Piskunov et al. 1995; Kupka et al. 1999) according to the spectral type of each target. These line lists orginally contain all lines with predicted line depths greater than 1%, assuming solar abundances. We proceeded to remove all hydrogen lines, lines that were blended with H lines, and lines that are strongly contaminated by telluric regions. We then automatically adjusted the line depths of each remaining line to provide the best fit to the observed Stokes *I* spectra.

Table 1. List of 21 archival spectropolarimetric observations of 9 PACWB, including the instrument used for the observations, date of observations and signal-to-noise ratio (SNR) in the Stokes I and V spectra.

Star	Instrument	Date	SNR I	SNR V
HD 36486	Narval	23.10.2008	5386	21947
	Narval	24.10.2008	6021	108758
HD 37468	ESPaDOnS	17.10.2008	3149	56388
HD 47839	Narval	10.12.2006	4416	19648
	Narval	15.12.2006	4528	37218
	Narval	09.09.2007	4497	25269
	Narval	10.09.2007	4384	33820
	Narval	11.09.2007	4280	24183
	Narval	20.10.2007	4545	39090
	Narval	23.10.2007	4563	41668
	ESPaDOnS	02.02.2012	4863	51425
HD 93250	HarpsPol	17.02.2013	4169	9523
HD 151804	HarpsPol	26.05.2011	6191	22047
HD 152408	ESPaDOnS	05.07.2012	843	12909
HD 164794	ESPaDOnS	19.06.2005	3083	14933
	ESPaDOnS	20.06.2005	3298	15249
	ESPaDOnS	23.06.2005	3118	15657
	HarpsPol	25.05.2011	5050	14081
	ESPaDOnS	14.06.2011	3346	29046
HD 167971	ESPaDOnS	30.06.2013	2671	22295
HD 190918	ESPaDOnS	25.07.2010	4096	13892

Using these final line masks, a mean wavelength of 5000 Å and a mean Landé factor of 1.2, we extracted LSD Stokes *I* and *V* profiles for each spectropolarimetric measurements. We also extracted LSD *N* polarisation profiles to check for spurious signatures. All LSD *N* profiles are flat, showing that the LSD *V* measurements do reflect the stellar magnetic field. The LSD *I* and Stokes *V* profiles of the 9 stars are shown in Fig. 1. LSD *V* profiles are also flat, showing no sign of a magnetic signature in any of the 9 PACWB.

3. LSD *I* profile fitting

To go further and evaluate the magnetic field in the studied PACWB, since PACWB are binary stars, we first needed to separate the individual spectra of each component in the LSD *I* profiles.

For each spectrum we fit the mean LSD Stokes *I* profile to determine the radial velocity $V_{\rm rad}$, the projected rotational broadening ($v \sin i$) and any contribution from non-rotational broadening that we consider to be macroturbulent broadening ($V_{\rm mac}$).

Ideally, fits to the observed profiles should be computed with Fourier techniques (e.g. Gray 2005; Simón-Díaz & Herrero 2014) directly on the intensity profiles (rather than the LSD profiles). However, this is very time consuming and not necessary here since the exact value of the parameters are not important for our purpose. We only need a good fit to the LSD profiles. Therefore, the profiles are computed as the convolution of a rotationally-broadened profile and a radial-tangential broadened profile following the parametrisation of Gray (2005), assuming equal contributions from the radial and tangential (RT) component. While this form of macroturbulence is not commonly used in the study of early-type stars (typically a Gaussian profile is used to characterise $V_{\rm mac}$), Simón-Díaz & Herrero (2014)

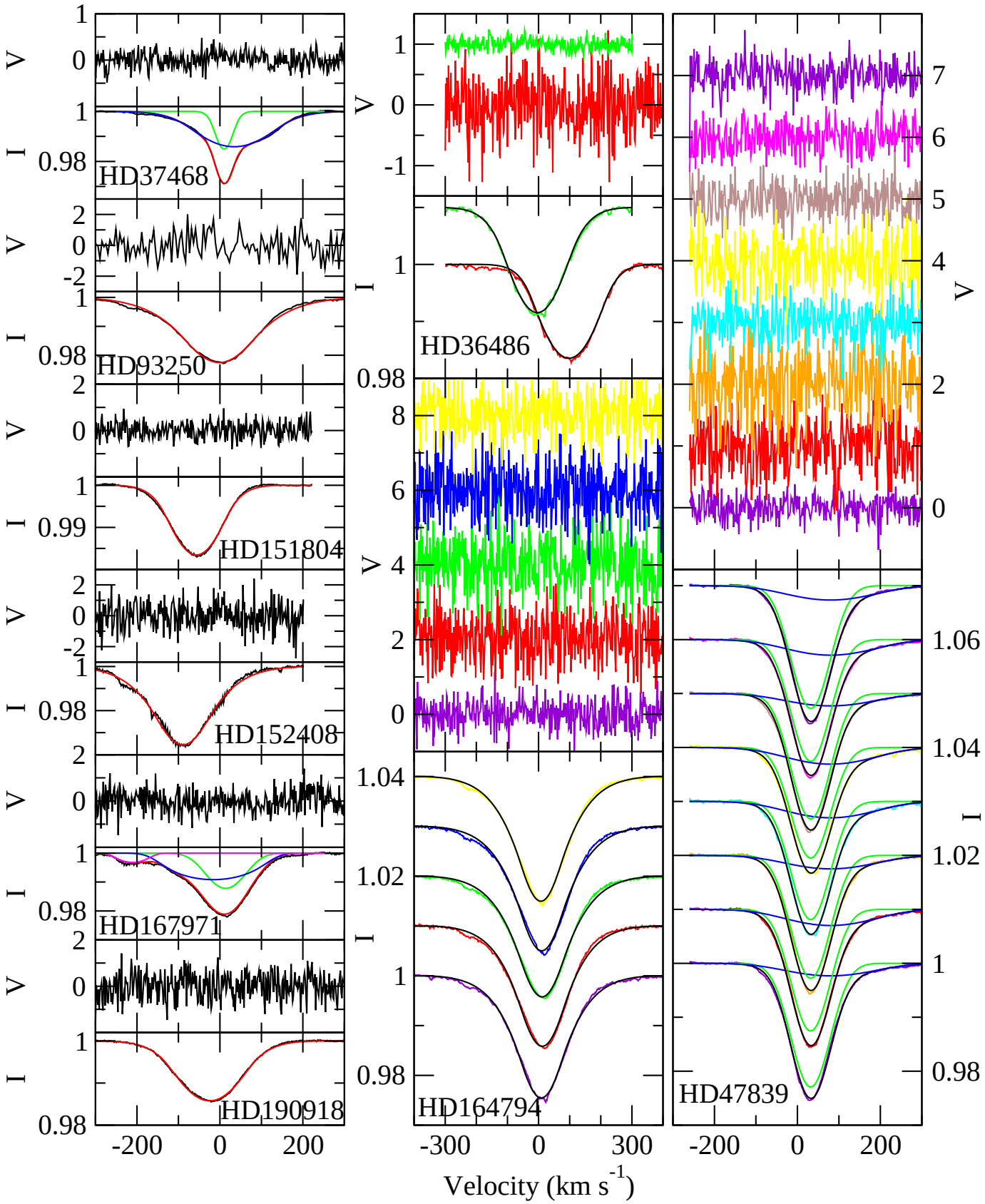


Fig. 1. LSD *I* (bottom panels) and Stokes *V* (top panels, y-axis multiplied by 10000) profiles of the 9 PACWB available in spectropolarimetric archives. When only one spectrum is available (left panels), observations are indicated in black and the fit in red. If several components are present the fit of the primary/secondary/tertiary component is shown in blue/green/pink, while the combined fit is in red. When several spectra are available for one star (middle and right panels), observations are indicated with various colours, and the fits are indicated in black with primary and secondary component fits indicated in green and blue respectively. In these cases, profiles are artificially shifted upwards to ease the reading.

Table 2. Parameters derived from the fit of LSD *I* profiles of each star. When several components are visible in the spectra, each component (primary, secondary and possibly tertiary) is fitted. The last column indicates the upper dipolar field strength limit in G for each spectrum.

Star HD	Date	Comp.	V_{rad} km s^{-1}	$v \sin i$ km s^{-1}	V_{mac} km s^{-1}	$B_{pol,max}$ G
36486	23.10.08		97	126	101	206
	24.10.08		-4	116	126	906
37468	17.10.08	prim	33	115	124	258
		sec	10	28	29	513
47839	10.12.06	prim	32	52	90	867
		sec	79	140	154	8579
	15.12.06	prim	32	52	90	472
		sec	79	140	154	4979
	09.09.07	prim	32	52	90	687
		sec	79	140	154	5581
	10.09.07	prim	32	52	90	543
		sec	79	140	154	4104
	11.09.07	prim	32	52	90	789
		sec	79	140	154	5658
	20.10.07	prim	32	52	90	449
		sec	79	140	154	3797
	23.10.07	prim	32	52	90	428
		sec	79	140	154	3837
	02.02.12	prim	32	52	90	337
		sec	79	140	154	3637
93250	17.02.13		-1.5	92	189	4367
151804	26.05.11		-58	79	83	850
152408	05.07.12		-91	69	154	1363
164794	19.06.05		12	76	180	1600
	20.06.05		10.5	75	191	1671
	23.06.05		9.5	71	191	1572
	25.05.11		8.9	71	186	1765
	14.06.11		6.7	69	189	865
167971	30.06.13	prim	13	63	73	1092
		sec	-16	146	62	1160
		ter	-212	52	36	-
190918	25.07.10		-25	102	111	1960

Table 3. Measured longitudinal field B_l and Null polarization N_l, with their error bars σ. When several components are visible in the spectra, the values were estimated for each component (primary, secondary and possibly tertiary).

Star HD	Date	Comp.	B_l G	N_l G	σ G
36486	23.10.08		43	13	38
	24.10.08		18	1	7
37468	17.10.08	prim	-3	35	19
		sec	16	-18	9
47839	10.12.06	prim	-27	17	25
		sec	-260	-173	210
	15.12.06	prim	-6	14	13
		sec	5	256	185
	09.09.07	prim	3	-13	20
		sec	-243	-173	210
	10.09.07	prim	8	7	15
		sec	-41	278	154
	11.09.07	prim	14	-14	23
		sec	-141	-95	211
	20.10.07	prim	-9	4	13
		sec	-98	146	140
	23.10.07	prim	-1	23	12
		sec	-27	-154	142
	02.02.12	prim	-6	-4	10
		sec	17	22	132
93250	17.02.13		-24	175	135
151804	26.05.11		-13	-34	33
152408	05.07.12		2	60	34
164794	19.06.05		-3	-18	52
	20.06.05		-2	44	52
	23.06.05		64	25	50
	25.05.11		6	87	54
	14.06.11		61	29	27
167971	30.06.13	prim	3	-16	40
		sec	98	16	59
		ter	-19	-216	115
190918	25.07.10		8	93	70

showed that it provides a good agreement with the Fourier techniques.

The code uses the MPFIT library (Moré 1978; Markwardt 2009) to find the best fit solution. Using a radial-tangential profile for V_{mac} tends to maximise $v \sin i$. Therefore the values we obtain for $v \sin i$ can be considered as upper limits.

For profiles that show obvious signs of spectroscopic companions (HD 37468, HD 47839 and HD 167971) we simultaneously fit multiple profiles, one for each component, to determine the overall best solution for the given SB2 (or SB3) profile. For HD 47839, since the various spectra show no significant variations, the averaged profile was fitted. The simultaneous fitting of multiple profiles for one spectrum is a difficult task and the solution is often degenerate. We therefore attempted to constrain each fit based on previous studies published in the literature whenever possible. For the other stars (SB1), only one component was fitted.

The various components and the resulting parameters are listed in Table 2. These parameters are only calculated to derive upper limits on the magnetic field strength. They should be used with care for other studies as they do not necessarily have a physical meaning. By running the fits several times with different initial guess values, and by visually comparing the quality of

the fit when changing the parameters, we estimate that the uncertainty on $v \sin i$ and $V_{\rm mac}$ is of the order of 10 km s^{-1}. The uncertainty on $V_{\rm rad}$ is of the order of a few km s^{-1}. The fits of each individual component, as well as the combined fit of all components, are shown in Fig. 1.

4. Magnetic field measurements

4.1. Longitudinal field measurement

From the LSD profiles we computed the longitudinal magnetic field (B_l) value and the corresponding null measurement N_l and their error bars σ, using the first-order moment method of Rees & Semel (1979) using the form given in Wade et al. (2000). We applied this measurement to the individual components of each stars, when visible.

The results are reported in Table 3. We find that the B_l and N_l values are all compatible with 0 within 3σ. This confirms that no field is detected in any of the 9 PACWB.

The magnetic field of one of our targets, HD 93250, has already been analysed with low-resolution FORS data by Nazé et al. (2012). They did not detect a magnetic field in this star neither, obtaining an even more stringent error bar of σ ~80 G.

4.2. Upper limit on undetected fields

Since we did not detect a magnetic field signature in the 9 PACWB we studied, we proceeded to determine the upper limit of the strength of a magnetic field that could have remain hidden in the spectral noise.

To this aim, for various values of the polar magnetic field $B_{\rm pol}$, we calculated 1000 oblique dipole models of each of the LSD Stokes V profiles with random inclination angle i and obliquity angle β, random rotational phase, and a white Gaussian noise with a null average and a variance corresponding to the SNR of each observed profile. Using the fitted LSD I profiles, we calculated local Stokes V profiles assuming the weak-field case and integrated over the visible hemisphere of the star. We obtained synthetic Stokes V profiles, which we normalised to the intensity continuum. We used the same mean Landé factor (1.2) and wavelength (5000 Å) as in the observations.

We then computed the probability of detection of a field in this set of models by applying the Neyman-Pearson likelihood ratio test (see e.g. Helstrom 1995; Kay 1998; Levy 2008) to decide between two hypotheses, H_0 and H_1, where H_0 corresponds to noise only, and H_1 to a noisy simulated Stokes V signal. This rule selects the hypothesis that maximises the probability of detection while ensuring that the probability of false alarm $P_{\rm FA}$ is not higher than a prescribed value considered acceptable. Following values usually assumed in the literature on magnetic field detections (e.g. Donati et al. 1997), we used $P_{\rm FA} = 10^{-3}$ for a marginal magnetic detection. We then calculated the rate of detections among the 1000 models for each of the profiles of the primary and secondary stars depending on the field strength (see Fig. 2).

We required a 90% detection rate to consider that the field should have statistically been detected. This translates into an upper limit for the possible undetected dipolar field strength for each star and spectrum. These upper limits are listed in Table 2. Since the computation of the upper limits rely on fitted I profiles, the uncertainty in the fits may introduce an error in the field strength we derive. Comparing limits derived from various fits of the same profile, we estimated that the error on the upper limits could be up to ~20%.

For the 3 PACWB for which each binary component has been fitted (HD 37468, HD 47839 and HD 167971), we provide an upper limit for each star. For the other 6 PACWB however, the result is contaminated by the undetected companion. For two of these PACWB, either the companion has never been detected (HD 151804) or it is known to be a faint cool star (HD 152804, see Mason et al. 1998), and therefore the contamination can be neglected. In the case of HD 190918, the companion is a Wolf-Rayet star which contributes to the spectrum with emission lines and continuum flux. Since the extracted LSD profile is normalized to the total continuum flux, it can be treated as a single star.

For HD 36486, HD 93250 and HD 164794 however, the contribution from the companion to the spectrum cannot be neglected. For HD 36486 and HD 93250, each component contributes to about 50% of the flux and the $v \sin i$ values of the primary and secondary are similar (see Harvin et al. (2002) for HD 36486 and Sana et al. (2011) for HD 93250). For these two stars, the upper limit values should thus be considered with care and are probably underestimated by a factor ~2. For HD 164794, the $v \sin i$ values of the two components are not very different neither (87 and 57 km s^{-1} according to Rauw et al. (2012)), but the secondary has deeper lines than the primary. For this star too, the upper limit value should thus be considered with care and might be significantly underestimated.

In addition, for stars for which several observations are available, statistics can be combined to extract a stricter upper limit taking into account that the field has not been detected in any of the observation, using the following equation:

$$P_{\rm comb} = 100 \left[1 - \prod_{i=1}^{n} \frac{(100 - P_i)}{100} \right],$$

where P_i is the detection probability for the ith observation, and $P_{\rm comb}$ is the detection probability for n observations combined. All probabilities are expressed in percents.

As an example, if two observations of one star were obtained with a detection probability of 80% and 90% respectively that no field stronger than 1000 G was detected, then the combined probability that such a 1000 G field was detected in none of the two observations would be 98%.

The final upper limit derived from this combined probability for each star for a 90% detection probability is listed in Table 4.

Finally, for one of our targets, HD 190918, using the same ESPaDOnS spectrum as in the present study, de la Chevrotière et al. (2014) checked for the presence of a magnetic field in the stellar wind from its emission lines. They detected no field and determined an upper limit on the wind magnetic field of 329 G for a 95.4% credible region using a Bayesian analysis. Their method assumes prior knowledge on the properties of the star, in particular a pole-on orientation for the magnetic geometry, and therefore leads to much more optimistic upper limits than the method presented here. The upper limit on the wind magnetic field they obtained can therefore not be directly compared to the upper limit on the stellar magnetic field we obtained here.

5. Discussion and conclusions

Parkin et al. (2014) showed that the surface magnetic field of the PACWB Cyg OB #9 would be between 0.3 and 52 G if one assumes simple magnetic field radial dependence, no or slow rotation, and a ratio of the energy density in the magnetic field to

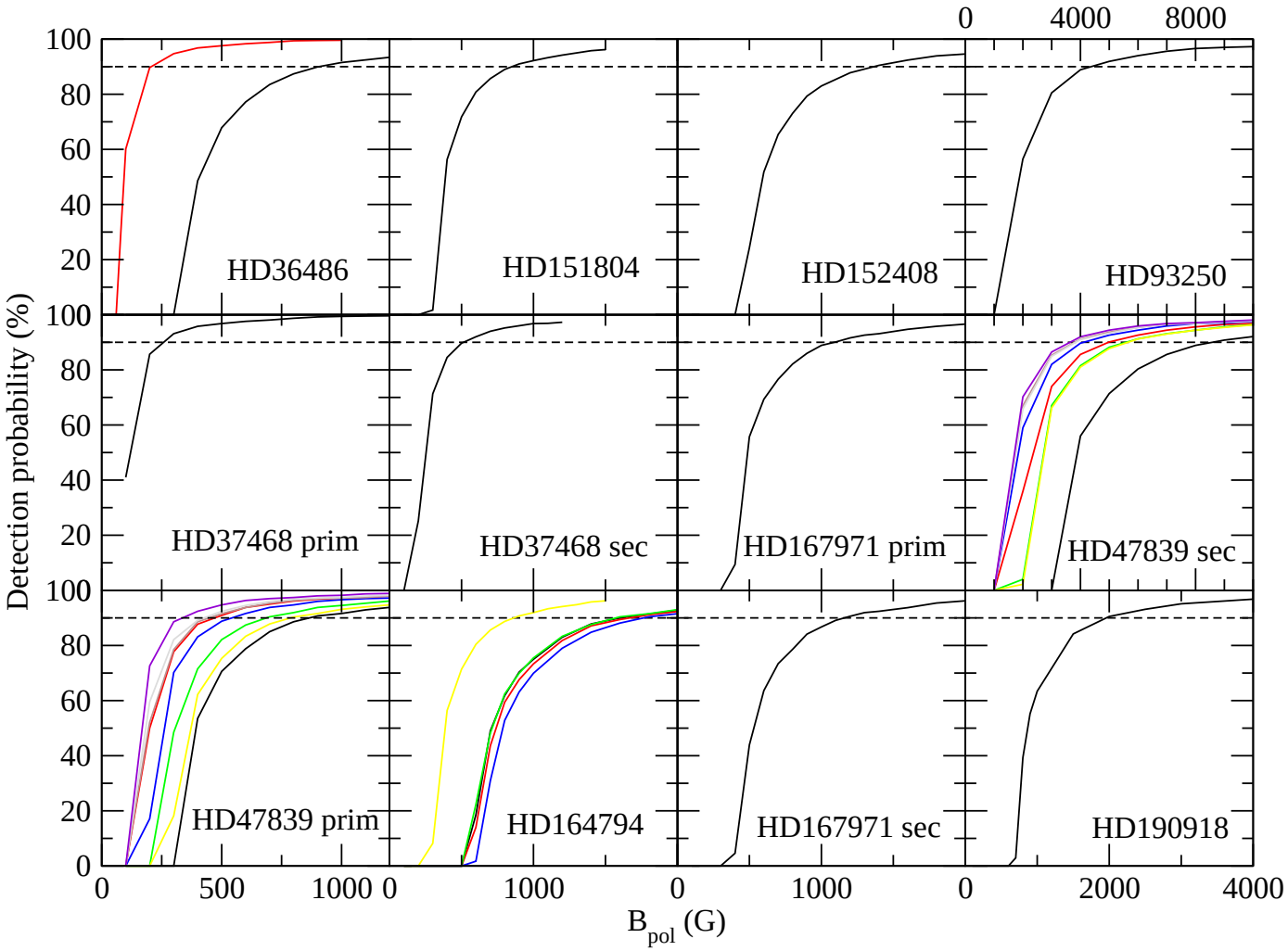


Fig. 2. Detection probability for each spectrum of each star as a function of the magnetic polar field strength. The horizontal dashed line indicates the 90% detection probability.

Table 4. Upper dipolar field strength limit in G, combining all available data for each detected component of each star.

Star	Component	$B_{\rm pol,max}$ G
HD 36486		203
HD 37468	prim	258
	sec	513
HD 47839	prim	178
	sec	1610
HD 93250		4367
HD 151804		850
HD 152408		1363
HD 164794		605
HD 167971	prim	1092
	sec	1160
	ter	-
HD 190918		1960

the local thermal energy density (ζ_B) of 5×10^{-5}, or between 30 and 5200 G if that ratio is assumed to be 0.5. In their work, the magnetic field strength scales with $\zeta_B^{1/2}$ and $V_{\rm rot}$.

The assumptions on the field configuration and slow rotation used by Parkin et al. (2014) are probably generally not adapted to PACWB. In particular, if the field is strong, the impact of the magnetic field on the wind, e.g. magnetic wind confinement, should be taken into account (ud-Doula & Owocki 2002; ud-Doula et al. 2008), and massive stars are often rapid rotators (e.g. Grunhut et al. 2013). Nevertheless, their work provides an idea of the typical field strengths that one might expect in PACWB.

Our analysis of archival spectropolarimetric data shows no magnetic detection in any of the 9 PACWB for which data are available. However, the precision reached by these archival observations is between 7 and 211 G for the measured longitudinal field. These values are typical of the precision reached for the measurements of fields in massive stars by the MiMeS collaboration (Grunhut et al., in prep.). Assuming an oblique dipole field, as observed in the vast majority of single massive stars, this leads to an upper limit of the undetected magnetic field at 3σ and a 90% probability of detection between 178 and 4367 G at the stellar pole, depending on the star.

While for some stars these archival observations are not really constraining (e.g. HD 93250), for several cases we can clearly exclude fields above 1000 G and thus large ζ_B values

are certainly not common in PACWB. The results obtained for HD 36486, HD 37468 and HD 47839 show that even dipolar fields above a few hundreds G, i.e. more moderate ζ_B, do not seem common in PACWB, while this corresponds to the typical field strength observed in magnetic massive stars (Petit et al. 2013). While the proportion of magnetic stars among OB stars (~7%) could fit with the proportion of PACWB among massive binary stars, our results clearly show that PACWB are not particularly magnetic compared to other massive stars. Therefore, no link could be established between the presence of a magnetic field typical of a magnetic massive star and the presence of synchrotron emission.

These archival data can however not exclude fields of a few tens of G or lower. Such field values would point towards low ζ_B values and would be sufficient to produce synchrotron emission. However, studies of magnetism in OB stars show that magnetic fields detected in these stars are always relatively strong (with B_l > 100 G). Weak magnetic fields are generally not found in massive stars, even when low detection thresholds are used. This is known as the magnetic dichotomy in massive stars (Aurière et al. 2007; Lignières et al. 2014).

However, ultra weak magnetic fields have recently been detected in some A stars (Lignières et al. 2009; Petit et al. 2011; Blazère et al. 2014). These fields could possibly also exist in higher mass stars, although attempts to detect them in B stars have been unsuccessful so far (Neiner et al. 2014; Wade et al. 2014a). Magnetic field amplification could exist in PACWB (Lucek & Bell 2000; Bell & Lucek 2001; Falceta-Gonçalves & Abraham 2012) and ultra weak stellar surface magnetic field could then be sufficient to produce synchrotron emission.

As a consequence, while this work represents the first ever effort to detect magnetic field signatures in PACWB, provide quantitative estimates of its possible value and constraints for models, and clearly excludes the presence of magnetic fields typical of massive stars as the origin of synchrotron emission in PACWB, more precise spectropolarimetric measurements of magnetic fields in PACWB are necessary before one can exclude the presence of very weak magnetic fields at the surface of PACWB stars. We plan to acquire such precise observations for very bright PACWB in the near future.

Nevertheless, even if ultra weak magnetic fields were present at the surface of PACWB and magnetic field amplification was at work, the question remains: if PACWB are not different, as far as their magnetic field is concerned, from typical massive stars, why are they particle accelerators? A possible scenario would be the production of a magnetic field at the location of the wind shock itself.

Acknowledgements. This research has made use of the SIMBAD database operated at CDS, Strasbourg (France), and of NASA's Astrophysics Data System (ADS). We thank the referee, M. Leutenegger, for his constructive feedback.

References

Aurière, M., Wade, G. A., Silvester, J., et al. 2007, A&A, 475, 1053
Bell, A. R. & Lucek, S. G. 2001, MNRAS, 321, 433
Blazère, A., Petit, P., Lignières, F., et al. 2014, ArXiv e-prints 1410.1412
Cazorla, C., Nazé, Y., & Rauw, G. 2014, A&A, 561, A92
De Becker, M., Pittard, J. M., Williams, P., & WR140 Consortium. 2011, Bulletin de la Societe Royale des Sciences de Liege, 80, 653
De Becker, M. & Raucq, F. 2013, A&A, 558, A28
de la Chevrotière, A., St-Louis, N., Moffat, A. F. J., & MiMeS Collaboration. 2014, ApJ, 781, 73
Donati, J.-F., Semel, M., Carter, B. D., Rees, D. E., & Collier Cameron, A. 1997, MNRAS, 291, 658
Dougherty, S. M., Pittard, J. M., Kasian, L., et al. 2003, A&A, 409, 217
Dzib, S. A., Rodríguez, L. F., Loinard, L., et al. 2013, ApJ, 763, 139
Falceta-Gonçalves, D. & Abraham, Z. 2012, MNRAS, 423, 1562
Farnier, C., Walter, R., & Leyder, J.-C. 2011, A&A, 526, A57
Gray, D. F. 2005, The Observation and Analysis of Stellar Photospheres (Cambridge University Press)
Grunhut, J. H., Wade, G. A., Leutenegger, M., et al. 2013, MNRAS, 428, 1686
Harvin, J. A., Gies, D. R., Bagnuolo, Jr., W. G., Penny, L. R., & Thaller, M. L. 2002, ApJ, 565, 1216
Helstrom, C. W. 1995, Elements of Signal Detection and Estimation (Prentice Hall)
Jardine, M., Allen, H. R., & Pollock, A. M. T. 1996, A&A, 314, 594
Kay, S. M. 1998, Fundamentals of Statistical Signal Processing, Volume 2: Detection Theory (Prentice Hall)
Kupka, F., Piskunov, N., Ryabchikova, T. A., Stempels, H. C., & Weiss, W. W. 1999, A&AS, 138, 119
Levy, B. C. 2008, Principles of Signal Detection and Parameter Estimation (Springer)
Lignières, F., Petit, P., Aurière, M., Wade, G. A., & Böhm, T. 2014, in IAU Symposium, Vol. 302, IAU Symposium, 338
Lignières, F., Petit, P., Böhm, T., & Aurière, M. 2009, A&A, 500, L41
Lucek, S. G. & Bell, A. R. 2000, MNRAS, 314, 65
Markwardt, C. B. 2009, in Astronomical Society of the Pacific Conference Series, Vol. 411, Astronomical Data Analysis Software and Systems XVIII, ed. D. A. Bohlender, D. Durand, & P. Dowler, 251
Mason, B. D., Gies, D. R., Hartkopf, W. I., et al. 1998, AJ, 115, 821
Moré, J. 1978, in Lecture Notes in Mathematics, Vol. 630, Numerical Analysis, ed. G. Watson (Springer Berlin Heidelberg), 105
Nazé, Y., Bagnulo, S., Petit, V., et al. 2012, MNRAS, 423, 3413
Neiner, C., Monin, D., Leroy, B., Mathis, S., & Bohlender, D. 2014, A&A, 562, A59
Parkin, E. R., Pittard, J. M., Nazé, Y., & Blomme, R. 2014, ArXiv e-prints 1406.5692
Petit, P., Lignières, F., Aurière, M., et al. 2011, A&A, 532, L13
Petit, V., Owocki, S. P., Wade, G. A., et al. 2013, MNRAS, 429, 398
Piskunov, N. E., Kupka, F., Ryabchikova, T. A., Weiss, W. W., & Jeffery, C. S. 1995, A&AS, 112, 525
Pittard, J. M., Dougherty, S. M., Coker, R. F., O'Connor, E., & Bolingbroke, N. J. 2006, A&A, 446, 1001
Rauw, G., Sana, H., Spano, M., et al. 2012, A&A, 542, A95
Rees, D. E. & Semel, M. D. 1979, A&A, 74, 1
Sana, H., de Mink, S. E., de Koter, A., et al. 2012, Science, 337, 444
Sana, H., Le Bouquin, J.-B., De Becker, M., et al. 2011, ApJ, 740, L43
Sana, H., Le Bouquin, J.-B., Lacour, S., et al. 2014, ArXiv e-prints 1409.6304
Simón-Díaz, S. & Herrero, A. 2014, A&A, 562, A135
ud-Doula, A. & Owocki, S. P. 2002, ApJ, 576, 413
ud-Doula, A., Owocki, S. P., & Townsend, R. H. D. 2008, MNRAS, 385, 97
Wade, G. A., Donati, J.-F., Landstreet, J. D., & Shorlin, S. L. S. 2000, MNRAS, 313, 851
Wade, G. A., Folsom, C. P., Petit, P., et al. 2014a, MNRAS, 444, 1993
Wade, G. A., Grunhut, J., Alecian, E., et al. 2014b, in IAU Symposium, Vol. 302, IAU Symposium, 265